This is an open access article published under a Creative Commons Attribution (CC-BY) License, which permits unrestricted use, distribution and reproduction in any medium, provided the author and source are cited.

ACS APPLIED MATERIALS & INTERFACES

Letter

www.acsami.org

Disordered Cellulose-Based Nanostructures for Enhanced Light Scattering

Soraya Caixeiro,*[,†] Matilda Peruzzo,[†,‡] Olimpia D. Onelli,[§] Silvia Vignolini,*[,§] and Riccardo Sapienza[†]

[†]Department of Physics King's College London, Strand, London WC2R 2LS, United Kingdom

[§]Department of Chemistry, Cambridge University, Lensfield Road, Cambridge CB2 1EW, United Kingdom

Supporting Information

ABSTRACT: Cellulose is the most abundant biopolymer on Earth. Cellulose fibers, such as the one extracted form cotton or woodpulp, have been used by humankind for hundreds of years to make textiles and paper. Here we show how, by engineering light−matter interaction, we can optimize light scattering using exclusively cellulose nanocrystals. The produced material is sustainable, biocompatible, and when compared to ordinary microfiber-based paper, it shows enhanced scattering strength (×4), yielding a transport mean free path as low as 3.5 μm in the visible light range. The experimental results are in a good agreement with the theoretical predictions obtained with a diffusive model for light propagation.

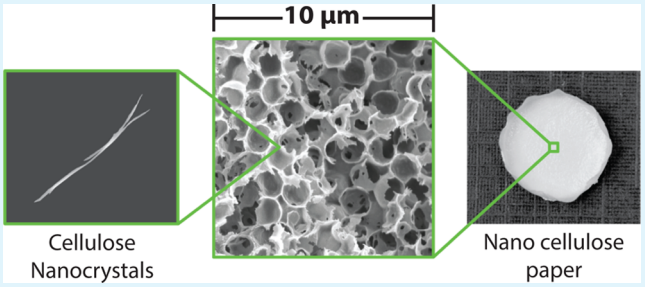

KEYWORDS: *cellulose nanocystals, photonics, scattering, photonic glass, diffusion, disorder*

INTRODUCTION

With the term "paper", we include a large variety of cellulose-based composite materials that find use in everyday life such as packaging and printing. Recently, paper-based technologies have captivated increasing interest not only due to their applications in sensing[1−3] and lasing,[4] but also in 3D cell scaffolding.[5] Cellulose can be easily functionalized to produce materials with enhanced mechanical, optical, and chemical properties because of its intrinsic fibrillary morphology and consequent porosity. These new materials are particularly attractive from an industrial point of view thanks to their low production costs.[6]

The main component of paper is cellulose.[7] Natural cellulose can be extracted from different sources: ranging from plants (such as wood pulp or cotton) to bacteria, to invertebrates and some marine animals,[8] nonetheless it is consistently found to have fibrillary nature.[9] Such natural fibers are generally composed of amorphous and crystalline regions, see Figure 1a. In the paper-manufacturing process, moist cellulose fibers extracted from natural sources are compressed together and dried. The thickness of the fibers and their packing density determine the optical response of the material.[7] Conventional fibers in paper are several tens of microns in diameter and therefore, they are not ideal to produce a strong scattering response, Figure 1b−d. By acid hydrolysis, a crystalline region, called cellulose nanocrystals (CNCs) can be extracted and suspended in water.[8] CNCs can be considered as rod-shaped colloidal particles typically 150 nm in length and a few nm in diameter[10] (Figure 1e), with a significantly high refractive index (about 1.55 in the visible range). CNCs have received an increase interest in photonics, because of their colloidal behavior and their ability to self-assemble into cholesteric optical films.[11,12]

Although CNCs have been intensively studied for structural color applications,[13] such materials have never been exploited to maximize scattering. Maximal scattering strength is, in fact, challenging to obtain. Optimal scattering design comes from the balance of scatterers' size, refractive index contrast and filling fraction. Therefore, it is fulfilled for dielectric particles of diameters comparable with the wavelength of light packed with maximal density assuring also a high refractive index contrast between the scatters and their surrounding environment.

Scattering is measured via the transport mean free path (l_t), the length beyond which the propagation is randomized, which for paper is typically of the order of 20 μm.[14] Maximal scattering, which means minimal l_t, is an important technological goal for producing whiter and more opaque materials. More efficient scattering implies that a smaller quantity of material is needed to achieve the same white coating.

Here, we report the bottom-up fabrication technique for the production of a new scattering paper-like material. Unlike conventional paper, our starting material is the smallest constituent of cellulose: the cellulose nanocrystal[11] (Figure 1a). We produce a nanostructure made solely of CNCs capable of improved light−matter interactions, due to its much smaller feature size (Figure 1e−g).

Received: December 13, 2016
Accepted: February 13, 2017
Published: February 13, 2017

 © 2017 American Chemical Society

DOI: 10.1021/acsami.6b15986
ACS Appl. Mater. Interfaces 2017, 9, 7885−7890

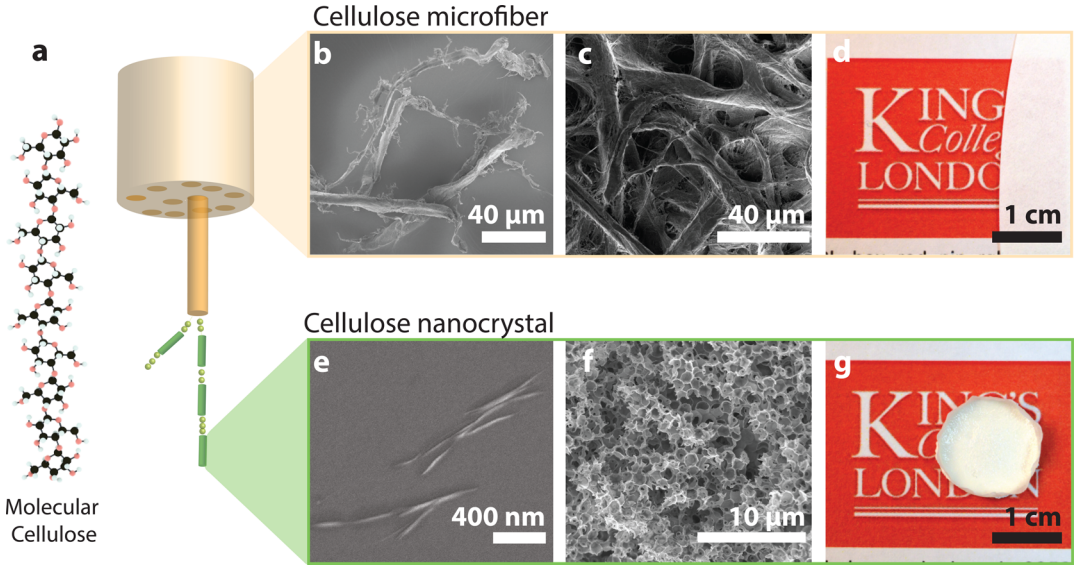

Figure 1. Structure and fabrication. A molecular chain of cellulose and a diagram showing the hierarchical structure of a cellulose chain is illustrated in panel a. Cellulose fiber is composed of fibrils (orange cylinder) with alternating crystalline (dark green rods) and amorphous (light green spheres) sections. On the top, (b) cellulose fibers used to fabricate (d) white paper whose fibrous structure is shown in (c) the SEM image. On the bottom, (e) cellulose nanocrystals that can be (g) self-assembled in the shape of a photonic glass structure by polystyrene sphere templating, and (f) the respective SEM image.

RESULTS

By characterizing the scattering response of the CNC-based photonic glass we obtain 400% stronger scattering than for standard cellulose fiber paper. The experimental results compare well with a diffusive model. Furthermore, we estimate the optimum fabrication conditions for maximum scattering and opacity, and point out a possible strategy to minimize costs.

A cellulose inverse photonic glass[15,16] is fabricated using a templating technique that consists in the codeposition of monodisperse PS spheres and CNCs and subsequential chemical etching of the PS spheres. This geometry is particularly convenient to optimize light-matter interaction because provides the right balance between the size of the scattering elements (at the edge of the spherical voids), and a high filling fraction.[16] Commercial cellulose nanocrystals (Forest Product Laboratory Canada) are extracted by sulfuric acid treatment of wood-pulp, leaving negative charged sulfate half-esters which are neutralized with Na^+ ions. The dimension of the colloids is around 5 nm in diameter and ranges from 150 to 200 nm in length. The pH of the suspension is neutral, whereas the surface change is 278 ± 1 mmol/kg estimated by conductometric titration.[17] The scanning electron microscope (SEM) image in Figure 1e shows the characteristic needlelike geometry of the CNCs.

A 4%wt CNCs aqueous solution (deionized water) is mixed with colloidal monodisperse polystyrene (PS) spheres of diameter d = 1.27 μm (Micro particles GmbH), such that the dry weight ratio between CNCs and PS spheres is 2:3, respectively. The obtained suspension is then cast into a hollow Teflon cylinder attached to a glass substrate with PS as in reference.[18] Prior to this, the Teflon cylinder is immerged in a NaOH bath to improve the hydrophilicity of its surfaces, while the glass is coated with PS to stabilize the film (to avoid cracking during drying).

The samples are kept in partially sealed containers and dried for 1−2 week(s) in a quasi-saturated water vapor atmosphere kept at a constant temperature (30 °C). Such conditions allow a slow evaporation rate which further improves the film quality by avoiding cracking and delamination. Once the sample is dry, the PS spheres are selectively etched in a bath of toluene for approximately 3−9 h, depending on the sample thickness (50−500 μm). Toluene also removes the PS coating substrate and separates the Teflon cylinder from the glass; this facilitates the detachment of the sample, yielding a free-standing cellulose inverse photonic glass, a nanostructured paper (Figure 1g). The CNCs properties are unaffected by the toluene bath,[19,20] as confirmed by the transmission experiments conducted for a timespan of over 10 h, showing no significant transmission change.

After the drying process, a random close-pack arrangement is formed, confirmed by SEM inspection (Figure 1f) and optically by the lack of iridescence and enhanced normal reflection. The only observable change is a minor reflection from the surface in contact with the glass i.e. where the cellulose layer is more compact. The resulting cellulose inverse photonic glass is shown in Figure 2. An SEM image of the structure reveals spherical voids of diameter around 1.3 μm (where the PS spheres were present prior to etching), as well as circular openings characteristic of a close packed structure, (in correspondence of the position where the PS spheres touched each other before template removal). We observe that such topology is homogeneous throughout the sample, as further confirmed by transmission studies on different areas of the sample (see later). In addition, a photograph of one of the samples fabricated is shown in Figure 1g (approximately 1.5 cm in diameter and 100 μm thick): the increased opaqueness of the photonic glass paper is visible even by the naked eye, when compared to conventional paper of similar thickness (Figure 1d).

We compare the scattering properties of CNCs photonic glass and common cellulose fiber paper by measuring l_t, by means of total transmission measurements (T) performed with an integrating sphere which collects the transmitted flux over all angles.[20] The measured light is sent to a spectrometer which

DOI: 10.1021/acsami.6b15986
ACS Appl. Mater. Interfaces 2017, 9, 7885−7890

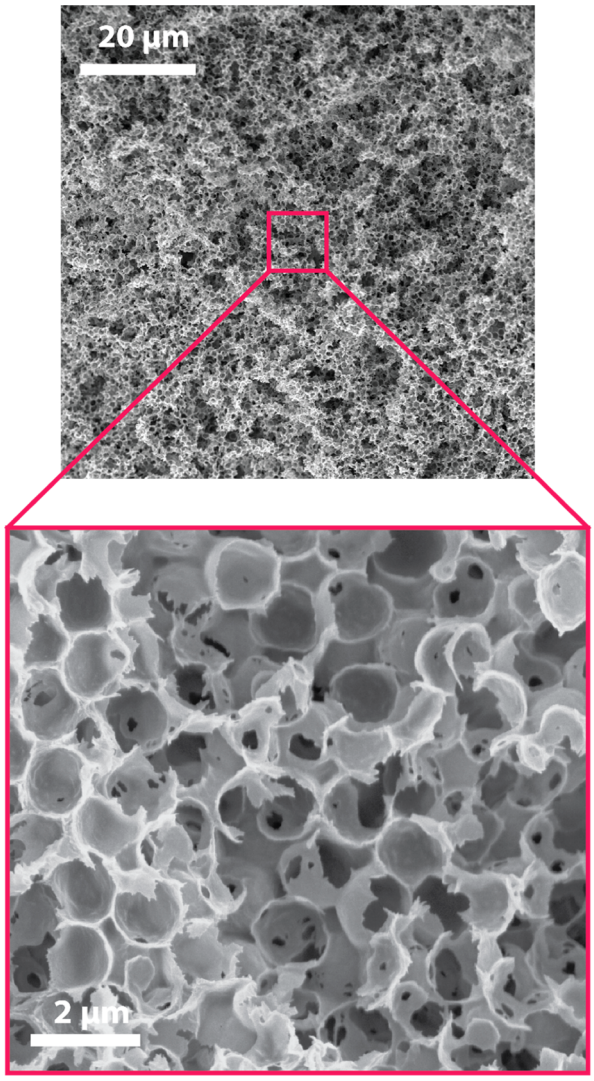

Figure 2. Sample morphology. The panel on the top reports an overview of the sample showing it is porous on a large scale. When imaged at higher magnification (bottom panel), it is possible to observe the micrometre-sized voids formed around the etched spheres. Smaller pores connecting the voids are visible, formed when the PS spheres were touching. The larger voids in the image are introduced when the sample is cut and prepared for SEM imaging.

provides spectral information. The photonic Ohm's law,[21,22] which is described by the change in total transmission (T) as a function of the sample thickness (L), is obtained via the stationary solution of the diffusion equation (assuming a slab geometry)[15,21]

$$T(L, \lambda) = \frac{1}{\alpha z_e} \frac{\sinh[\alpha(z_p + z_e)]\sinh(\alpha z_e)}{\sinh[\alpha(L + 2z_e)]} \quad (1)$$

where $\alpha = 1/l_a$ is the reciprocal of the absorption length l_a, z_e is the extrapolation length and z_p is the penetration length, typically taken to be equal with $z_e = \frac{1}{2\alpha}\ln\left(\frac{1+\alpha z_0}{1-\alpha z_0}\right)$ and $z_0 = \frac{2}{3} l_t \frac{1+R}{1-R}$. R is the averaged reflectivity ($R = 0.39$ assuming a filling fraction of ~55% and $n = 1.55$).

The microfiber paper used is Whatman filter paper, grade 1, with a reported thickness of 180 μm confirmed by SEM inspection. While for the paper photonic glass it was possible to produce samples of different thicknesses, for cellulose fiber paper multiple sheets of paper had to be compressed together in order to increase the overall thickness. The transmission spectra of cellulose fiber paper, averaged over 3 measurements, were fitted with eq 1 for each wavelength as shown in Figure 3a

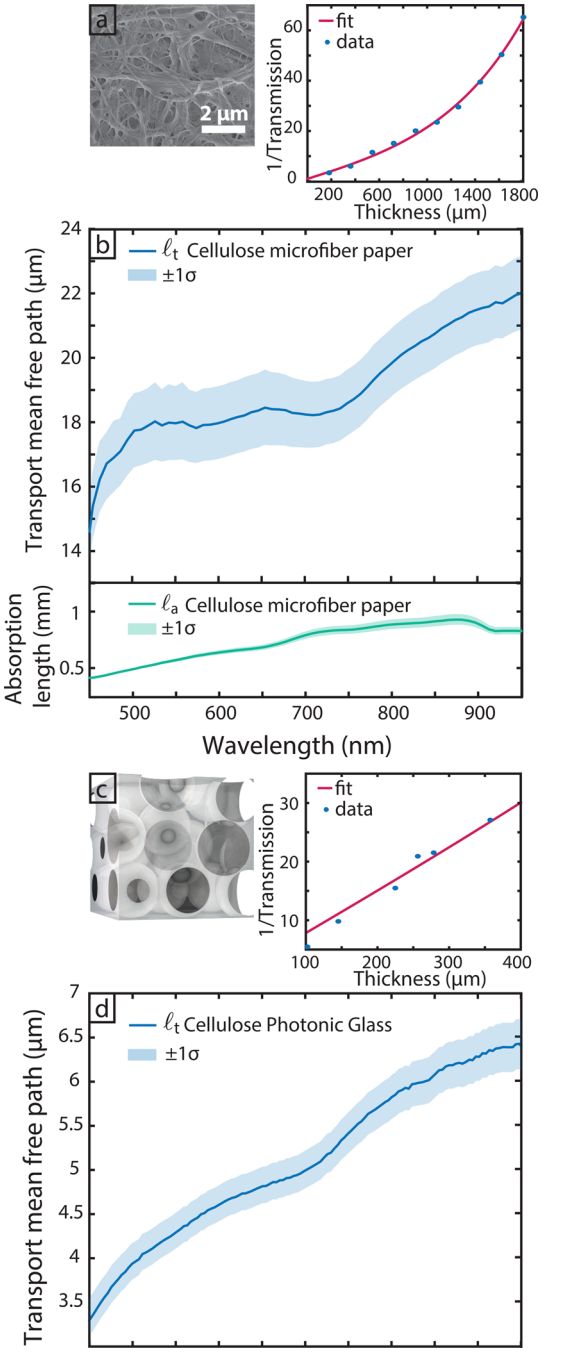

Figure 3. Measured scattering strength. (a) Cellulose microfibre paper SEM and fit of the total transmission data at different thicknesses (λ = 600 nm). (b) Measurement of the light transport mean free path (blue) and absorption length (green) for microfiber paper. The error bars are shown by the shaded area around the lines, for both fitting parameters. (c) Model of structure of a cellulose inverse photonic glass and fit of the total transmission data at different thicknesses (λ = 600 nm). (d) Measurements of the light transport mean free path for the inverse cellulose photonic glass. The error bars are shown by the blue shaded area around the line.

DOI: 10.1021/acsami.6b15986
ACS Appl. Mater. Interfaces 2017, 9, 7885−7890

and b. A typical fit at λ = 600 nm is plotted in Figure 3a highlighting the exponential dependence of the inverse transmission $(1/T)$ on the thickness (L) due to absorption. Here, l_t and l_a are estimated by a two-parameter fit of eq 1. We use a multistep fitting routing: 1. l_t and l_a are taken as free parameters of the fit to obtain approximate values for each wavelength; 2. each parameter is fitted independently using the other parameter as an input, until convergence is achieved (after 4 iterations). Furthermore, the fitted value from each wavelength is used as the starting point of the consequent one to improve the convergence. The measured l_t ranges between 15 and 22 μm in the visible spectra as depicted in Figure 3b), whereas l_a is of the order of a millimeter. The measured l_t is an underestimation of the actual value, although the air gaps between the sheets are expected to increase the apparent l_t, we estimate by microscopy inspection that they are less than 10% of the sample thickness. The reflection at each interface (about 40% for each sheets), on the other hand, is a more significant effect that increases the total reflectivity, thus lowering the transmission and increasing the measured l_t.

The measurement of l_t in the case of the photonic glass paper was performed by comparing samples with different thicknesses (Figure 3c) in the range 100−400 μm. Such thicknesses are estimated by SEM. The values of the thickness are averaged over different areas on the sample, with an error of around 5%. The transmission spectra of the cellulose photonic glass are averaged over different regions of the sample and a dispersion less than 5% is measured. Using the same procedure depicted above, the data is fitted with eq 1. As l_a in these samples is much larger than the sample thickness, lossless Ohm's law is valid, as shown in Figure 3c. Therefore, for simplicity and stability of the fit, we choose α = 0. Figure 3d shows l_t obtained as a function of wavelength. The statistical error of the fit, accredited to minor sample-to-sample variation, is estimated to be less than 10%. As expected, l_t decreases toward shorter wavelengths as predicted by Mie theory (see later). The measured l_t is in the range $l_t \approx 3-7$ μm for the visible range with very shallow resonances. The lack of resonances is expected, as air voids in a higher refractive index matrix are poor resonators, in contrast with high refractive index spheres which show appreciably stronger resonances.[15,18] The scattering strength of the photonic glass paper is significantly stronger: l_t is 4 times smaller than that measured for cellulose fiber paper.

The theoretical calculations are performed via Mie theory and independent scattering approximation, taking into account the polydispersity of the PS spheres.[23,24] Comparing to previous work[16] we expect the photonic glass paper to have a filling fraction around f = 50−55%, smaller than the theoretical limit for hard-sphere random packing.[25] The comparison between the theoretical results for different degrees of polydispersity is shown in Figure 4. Because the resonances are weak, they are unaffected by the small polydispersity.

We use the Mie model to investigate the optimum void diameter required to maximize scattering. Figure 5 plots l_t for different void diameters (at a wavelength of λ = 600 nm), both in the absence of polydispersity and at 2% polydispersity. At d = 250 nm, l_t is at its lowest value, around 1.3 μm, whereas for smaller diameters, l_t increases rapidly for decreasing d, as dictated by Rayleigh scattering. Although scattering may be increased by using smaller PS sphere to nanostructure the CNCs, smaller CNCs than the ones used here are required to ensure maximal close-packing of the sphere and consequently stronger scattering and a lower l_t.

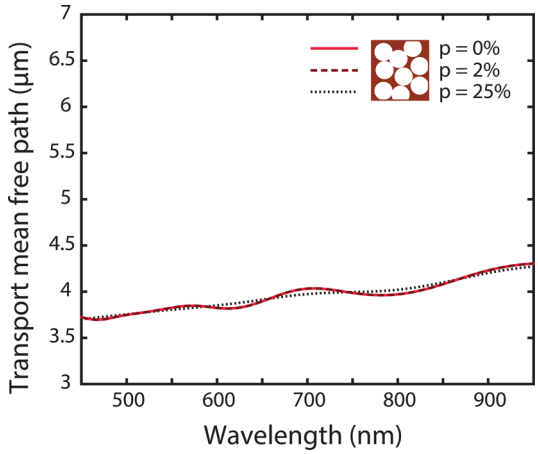

Figure 4. Modeling experimental results. Theoretical transport mean free path calculated for air spheres in cellulose matrix $n_{cellulose}$ = 1.55 at a filling fraction of f = 0.55 as a function of wavelength (full red line) assuming polydispersity of 2% (dashed red line) and assuming a polydispersity of 25% (dashed black line).

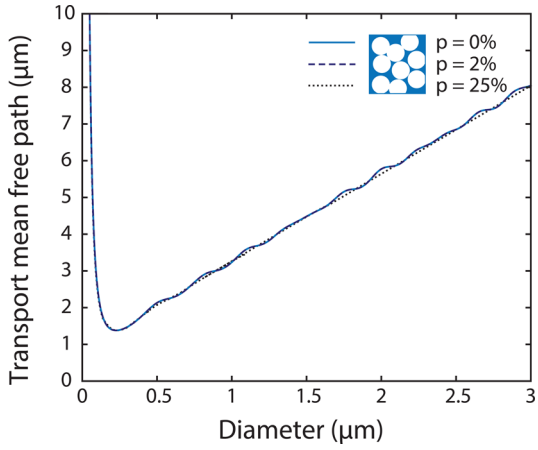

Figure 5. Theoretical scattering strength with different void diameter. Theoretical transport mean free path calculated for air spheres in cellulose matrix $n_{cellulose}$ = 1.55 at a filling fraction of f = 0.55, as a function of different void diameters at λ = 600 nm.

Polydisperse PS spheres are cheaper and easier to produce than its monodisperse counterpart, therefore we explore here the effect of polydispersity in the templating matrix. Our calculations show that even for large polydispersity, as high as 25%, the average value of l_t is unaffected, only the resonances are damped, as shown by the dotted black line in Figure 4 and 5.

CONCLUSIONS

In conclusion, we have presented a highly scattering nanostructured CNCs paper with l_t = 3−7 μm. The inverse photonic glass made of CNC scatters 4 times more than standard cellulose fiber paper. By post-treatment of the film, or by adding other materials in suspension, the properties of the produced photonic glass can be further improved in terms of mechanical properties and moisture-resistance.[26−29] Increased scattering implies that the same visual contrast and whiteness can be achieved in a thinner sample. With a simple theoretical model, we identify the optimum sphere diameter of about half

DOI: 10.1021/acsami.6b15986
ACS Appl. Mater. Interfaces 2017, 9, 7885−7890

the light wavelength, for which the scattering strength can be maximized. Large scattering strength allows for larger contrast in sensors, thinner paper, which would reduce coating and packaging. Furthermore, nanophotonic enhanced paper offers the additional benefit of large porosity together with increased light−matter interaction.

■ ASSOCIATED CONTENT

Supporting Information

The Supporting Information is available free of charge on the ACS Publications website at DOI: 10.1021/acsami.6b15986.

Additional figure (PDF)

■ AUTHOR INFORMATION

Corresponding Authors

*E-mail: soraya.carlos_caixeiro@kcl.ac.uk.
*E-mail: sv319@cam.ac.uk.

ORCID

Soraya Caixeiro: 0000-0003-4605-957X
Olimpia D. Onelli: 0000-0002-8720-2179

Present Address

‡M.P. is currently at Institute of Science and Technology Austria (IST Austria), 3400 Klosterneuburg, Austria

Notes

The authors declare no competing financial interest.

■ ACKNOWLEDGMENTS

The authors thank Michele Gaio, Giulia Guidetti, and Bruno Frka-Petesic for the fruitful discussions. This research was funded by the EPSRC (EP/M027961/1), the Leverhulme Trust (RPG-2014-238), Royal Society (RG140457), the BBSRC David Phillips fellowship (BB/K014617/1), and the European Research Council (ERC-2014-STG H2020 639088). All data created during this research are provided in full in the results section and Supporting Information. They are openly available from figshare and can be accessed at ref 30.

■ REFERENCES

(1) Nie, Z.; Nijhuis, C. A.; Gong, J.; Chen, X.; Kumachev, A.; Martinez, A. W.; Narovlyansky, M.; Whitesides, G. M. Electrochemical Sensing in Paper-based Microfluidic Devices. *Lab Chip* **2010**, *10*, 477−483.

(2) Delaney, J. L.; Hogan, C. F.; Tian, J.; Shen, W. Electrogenerated Chemiluminescence Detection in Paper-Based Microfluidic Sensors. *Anal. Chem.* **2011**, *83* (4), 1300−1306.

(3) Yan, C.; Wang, J.; Kang, W.; Cui, M.; Wang, X.; Foo, C. Y.; Chee, K. J.; Lee, P. S. Highly Stretchable Piezoresistive Graphene-Nanocellulose Nanopaper for Strain Sensors. *Adv. Mater.* **2014**, *26*, 2022−2027.

(4) Derda, R.; Laromaine, A.; Mammoto, A.; Tang, S. K. Y.; Mammoto, T.; Ingber, D. E.; Whitesides, G. M. Paper-supported 3D Cell Culture for Tissue-based Bioassays. *Proc. Natl. Acad. Sci. U. S. A.* **2009**, *106* (44), 18457−18462.

(5) Viola, I.; Ghofraniha, N.; Zacheo, A.; Arima, V.; Conti, C.; Gigli, G. Random Laser Emission from a Paper-based Device. *J. Mater. Chem. C* **2013**, *1*, 8128−8133.

(6) Moon, R. J.; Martini, A.; Nairn, J.; Simonsen, J.; Youngblood, J. Cellulose Nanomaterials review: Structure, properties and Nanocomposites. *Chem. Soc. Rev.* **2011**, *40*, 3941−3994.

(7) Hubbe, M. A.; Pawlak, J. J.; Koukoulas, A. A. Paper's appearance: A review. *BioResources* **2008**, *3* (2), 627−665.

(8) Habibi, Y.; Lucia, L. A.; Rojas, O. J. Cellulose Nanocrystals: Chemistry, Self-assembly, and Applications. *Chem. Rev.* **2010**, *110* (6), 3479−3500.

(9) Eichhorn, S. J.; Dufresne, A.; Aranguren, M.; Marcovich, N. E.; Capadona, J. R.; Rowan, S. J.; Weder, C.; Thielemans, W.; Roman, M.; Renneckar, S.; Gindl, W.; Veigel, S.; Keckes, J.; Yano, H.; Abe, K.; Nogi, M.; Nakagaito, A. N.; Mangalam, A.; Simonsen, J.; Benight, A. S.; Bismarck, A.; Berglund, L. A.; Peijs, T. Review: Current International Research into Cellulose Nanofibres and Nanocomposites. *J. Mater. Sci.* **2010**, *45*, 1−33.

(10) Mariano, M.; El Kissi, N.; Dufresne, A. Cellulose Nanocrystals and Related Nanocomposites: Review of some Properties and Challenges. *J. Polym. Sci., Part B: Polym. Phys.* **2014**, *52*, 791−806.

(11) Fernandes, S. N.; Almeida, P. L.; Monge, N.; Aguirre, L. E.; Reis, D.; de Oliveira, C. L. P.; Neto, A. M. F.; Pieranski, P.; Godinho, M. H. Mind the Microgap in Iridescent Cellulose Nanocrystal Films. *Adv. Mater.* **2017**, *29*, 1603560.

(12) Shopsowitz, K. E.; Qi, H.; Hamad, W. Y.; MacLachlan, M. J. Free-standing Mesoporous Silica Films with Tunable Chiral Nematic structures. *Nature* **2010**, *468*, 422−425.

(13) Middleton, R.; Steiner, U.; Vignolini, S. In *Bio-inspired Polymers*; Bruns, N., Kilbinger, A. F. M., Eds.; The Royal Society of Chemistry: Croydon, U.K., 2017; Chapter 17, pp 555−585.

(14) Burresi, M.; Cortese, L.; Pattelli, L.; Kolle, M.; Vukusic, P.; Wiersma, D. S.; Steiner, U.; Vignolini, S. Bright-white Beetle Scales Optimise Multiple Scattering of light. *Sci. Rep.* **2014**, *4*, 6075.

(15) Garcia, P. D.; Sapienza, R.; Bertolotti, J.; Martín, M. D.; Blanco, Á.; Altube, A.; Viña, L.; Wiersma, D. S.; López, C. Resonant Light Transport through Mie Modes in Photonic Glasses. *Phys. Rev. A: At., Mol., Opt. Phys.* **2008**, *78*, 023823.

(16) Garcia, P. D.; Sapienza, R.; Blanco, Á.; López, C. Photonic Glass: A Novel Random Material for Light. *Adv. Mater.* **2007**, *19*, 2597−2602.

(17) Beck, S.; Methot, M.; Bouchard, J. General Procedure for Determining Cellulose Nanocrystal Sulfate Half-Ester Content by Conductometric Titration. *Cellulose* **2015**, *22*, 101−116.

(18) Caixeiro, S.; Gaio, M.; Marelli, B.; Omenetto, F. G.; Sapienza, R. Silk-Based Biocompatible Random Lasing. *Adv. Opt. Mater.* **2016**, *4* (7), 998−1003.

(19) Heux, L.; Chauve, G.; Bonini, C. Nonflocculating and Chiral-Nematic Self-ordering of Cellulose Microcrystals Suspensions in Nonpolar Solvents. *Langmuir* **2000**, *16* (21), 8210−8212.

(20) Frka-Petesic, B.; Jean, B.; Heux, L. First Experimental Evidence of a Giant Permanent Electric-dipole Moment in Cellulose Nanocrystals. *EPL* **2014**, *107*, 28006.

(21) Garcia, N.; Genack, A. Z.; Lisyansky, A. A. Measurement of the Transport Mean Free Path of Diffusing Photons. *Phys. Rev. B: Condens. Matter Mater. Phys.* **1992**, *46*, 14475.

(22) Durian, D. J. Influence of Boundary Reflection and Refraction on Diffusive Photon Transport. *Phys. Rev. E: Stat. Phys., Plasmas, Fluids, Relat. Interdiscip. Top.* **1994**, *50*, 857−866.

(23) Bohren, C. F.; Huffman, D. In *Absorption and Scattering of Light by Small Particles*; Wiley: New York, 1983.

(24) Gaio, M.; Peruzzo, M.; Sapienza, R. Tuning Random Lasing in Photonic Glasses. *Opt. Lett.* **2015**, *40* (7), 1611−1614.

(25) Song, C.; Wang, P.; Makse, H. A. A Phase Diagram for Jammed Matter. *Nature* **2008**, *453*, 629−632.

(26) Giese, M.; Blusch, L. K.; Khan, M. K.; Hamad, W. Y.; MacLachlan, M. J. Responsive Mesoporous Photonic Cellulose Films by Supramolecular Cotemplating. *Angew. Chem., Int. Ed.* **2014**, *53*, 8880−8884.

(27) Guidetti, G.; Atifi, S.; Vignolini, S.; Hamad, W. Y. Flexible Photonic Cellulose Nanocrystal Films. *Adv. Mater.* **2016**, *28* (45), 10042−10047.

(28) Gicquel, E.; Martin, C.; Yanez, J. G.; Bras, J. Cellulose Nanocrystals as New Bio-based Coating Layer for Improving Fiber-based Mechanical and Barrier Properties. *J. Mater. Sci.* **2017**, *52* (6), 3048−3061.

DOI: 10.1021/acsami.6b15986
ACS Appl. Mater. Interfaces 2017, 9, 7885−7890

(29) Rodionova, G.; Lenes, M.; Eriksen, O.; Gregersen, O. Surface Chemical Modification of Microfibrillated Cellulose: Improvement of Barrier Properties for Packaging Applications. *Cellulose* **2011**, *18*, 127−134.
(30) Caixeiro, S.; Peruzzo, M.; Onelli, O. D.; Vignolini, S.; Sapienza, R. Disordered Cellulose-based Nanostructures for Enhanced Light-scattering. *ACS Appl. Mater. Interfaces* **2017**, DOI: 10.1021/acsami.6b15986. See Figshare DOI: 10.6084/m9.figshare.4598239.

DOI: 10.1021/acsami.6b15986
ACS Appl. Mater. Interfaces 2017, 9, 7885−7890